(x,y,z) at the center, apart from the outer pair of signals (z), separated by $4D'$ and the inner pair (x,y) spaced by $2D'$. Evidently, in the case of **3–5**, such an absorption would be masked by that of the doublet trianions $\mathbf{3}^{\bullet 3-}$–$\mathbf{5}^{\bullet 3-}$. Thus, prospects to detect the corresponding quartet trianions of **3–5** are rather dim.

Conclusions

The subsequent reduction steps leading to paramagnetic mono-, di-, and trianions are schematically depicted for **3–5** in Figure 6. These species have been characterized as follows:

(i) *Radical (doublet) anions*, $\mathbf{3}^{\bullet -}$–$\mathbf{5}^{\bullet -}$, with one unpaired electron in a lateral π-system. Electron exchange with the second equivalent system is fast on the hyperfine time scale, except under conditions of tight ion pairing.

(ii) *Triplet dianions*, $\mathbf{3}^{\bullet\bullet 2-}$–$\mathbf{5}^{\bullet\bullet 2-}$, with two unpaired electrons, one in each of the two lateral π-systems. Experimental evidence suggests a simultaneous presence of singlet dianions in which the two electrons are paired.[27]

(iii) *Radical (doublet) trianions*, $\mathbf{3}^{\bullet 3-}$–$\mathbf{5}^{\bullet 3-}$, with two paired electrons, in each of the lateral π-systems and one unpaired electron in the central phane unit. Simultaneous occurrence of quartet trianions, with three unpaired electrons, could not be confirmed experimentally.

This interpretation is in full accord with the cyclic voltammogram of **5**-tBu$_4$.[9a] The first two reversible reduction waves of this compound appear at $E_{1/2}^{(1)} = -2.54$ V (neutral $\xrightleftharpoons{+e^-}$ monoanion) and $E_{1/2}^{(2)} = -2.61$ V (monoanion $\xrightleftharpoons{+e^-}$ dianion), i.e., close to the potential $E_{1/2}^{(1)}$ of the terphenyl **7** (−2.62 V), whereas a third, likewise reversible, wave is observed at $E_{1/2}^{(3)} = -2.80$ V (dianion $\xrightleftharpoons{+e^-}$ trianion). The finding that this $E_{1/2}^{(3)}$ value of **5**-tBu$_4$ is somewhat more negative than the potential $E_{1/2}^{(1)}$ of the dibenzocyclophane **2** (−2.68 V) can readily be rationalized in terms of the two negative charges that are present in the lateral π-systems of **5**-tBu$_4$ at the uptake of an additional electron by the central phane unit (Figure 6).

(27) Due to an excessive line broadening, the NMR spectra of the singlet dianions could not be reliably analyzed (see above), so that the charge distribution in these diamagnetic species has not been established unequivocally. As indicated in Figure 6, it is assumed that each of the two lateral π-systems accommodates one negative charge. Such a structure is considered to be favored by electrostatic repulsion and it also complies with the spin distributions in the corresponding radical anions and, particularly, in the radical trianions. However, an alternative structure with both electrons occupying, at least temporarily, only one of the lateral π-systems cannot be completely ruled out in default of direct experimental evidence.

Experimental Section

The syntheses of **3**,[4a,c] **4**,[4a,c] **5**,[4b] and **5**-tBu$_4$[4c] have been reported; a detailed description will be given in a forthcoming paper.[4d] **3**-d_2 was prepared by a procedure analogous to that used for **3**,[4a,c] with the reagent styrene being replaced by its p-deuterio derivative.

***p*-Deuteriostyrene.** A 2.2 M solution of n-butyllithium (22 mL, 48.4 mmol) in n-hexane was added at −108 °C to a solution of p-bromostyrene (8.0 g, 43.5 mmol) in a mixture of THF, diethyl ether, and n-hexane (60 mL, 4:1:1). After 5 min, deuterium oxide (2 mL, 100 mmol) was admitted; the reaction mixture was warmed to room temperature and, following an addition of ice-water (50 mL), it was diluted with diethyl ether (200 mL). The organic layer was washed with a saturated solution of ammonium chloride (2 × 100 mL) and water and dried over magnesium sulfate. The solvent was evaporated and the residue distilled, yielding 3.66 g (80%) of p-deuteriostyrene: bp 72 °C (100 mmHg); ^{1}H NMR δ 5.23 (dd, ^2J = 1.1 Hz, $^3J_{cis}$ = 11 Hz, 1 H, H-2′ cis), 5.75 (dd, $^3J_{trans}$ = 18 Hz, 1 H, H-2′trans), 6.72 (dd, 1 H, H-1′), 7.32 and 7.42 (dd, ^3J = 8 Hz, 4 H, Ar-H); MS, m/e (relative intensity) 105 (M^+, 100), 104 (27), 79 (17), 78 (13).

4′,5″-Bis(*p*-deuteriophenyl)dibenzo[2.2]paracyclophane-1,9-diene (3-d_2). 1,9(10)-Dibromo[2.2]paracyclophane-1,9-diene (1.0 g, 1.76 mmol reacted with 1.5 mL (15.9 mmol) of p-deuteriostyrene to yield 800 mg (71%) of 1,9(10)-bis[2′-(*E*)-p-deuteriostyryl][2.2]paracyclophane-1,9-diene.[4a,c] Reaction of this compound (800 mg, 1.96 mmol) with propynal (400 mg, 7.4 mmol) afforded 220 mg (22%) of 5′,5″-bis(p-deuteriophenyl)dibenzo[2.2]paracyclophane-1,9-diene-4′,4″-dicarbaldehyde and 250 mg (25%) of 4″,5′-bis(p-deuteriophenyl)dibenzo[2.2]paracyclophane-1,9-diene-4′,5″-dicarbaldehyde. Decarbonylation of the latter gave 67 mg (30%) of **3**-d_2 with a deuterium content in the two para positions better than 90% (according to ^{1}H NMR).

All paramagnetic species obtained by reduction with potassium in an ethereal solvent were persistent at temperatures below 263 K.

The ESR spectra were taken on a Varian-E9 instrument, while a Bruker ESP-300 system served for the ENDOR and TRIPLE-resonance studies.

Acknowledgment. We are greatly obliged to Prof. M. Rabinovitz, The Hebrew University of Jerusalem, Israel, and K. Müllen, Johannes Gutenberg—Universität Mainz, F.R.G., in whose laboratories the NMR studies of the reduction products of **2**, **3**, and **5** were carried out. Our thanks are also due to Prof. J. Heinze, University of Freiburg, F.R.G. for communicating his cyclic voltammetric data to us prior to publication. Financial support by the Swiss National Science Foundation and the German Fonds der Chemischen Industrie is greatfully acknowledged. B.K. and O.R. are indebted to the Studienstiftung des Deutschen Volkes for graduate fellowships.

Hydrogen–Deuterium-Exchange Reactions of Methoxide–Methanol Clusters

S. E. Barlow, Thuy Thanh Dang, and Veronica M. Bierbaum*

Contribution from the Department of Chemistry and Biochemistry, University of Colorado, Boulder, Colorado 80309-0215. *Received January 10, 1990*

Abstract: The tandem flowing afterglow-selected ion flow tube has been employed to measure rate coefficients for a series of 12 bimolecular isotope-exchange reactions of methoxide–methanol clusters. From these kinetic measurements the dissociation energies of several hydrogen-bonded dimers were determined: $CH_3O^-\cdot DOCH_3$ (28.3 ± 0.1 kcal/mol), $CH_3O^-\cdot HOCD_3$ (28.5 ± 0.1 kcal/mol), $CH_3O^-\cdot DOCD_3$ (28.1 ± 0.1 kcal/mol) $CD_3O^-\cdot HOCD_3$ (28.9 ± 0.1 kcal/mol), and $CD_3O^-\cdot DOCD_3$ (28.5 ± 0.1 kcal/mol). Differences in the bond strengths of these cluster ions can be understood in terms of the acidity of the neutral molecule and the basicity of the anion involved in the cluster; a given ion makes a stronger bond with a stronger acid while a given neutral molecule makes a stronger bond with a stronger base. By use of literature values of the electron affinity of the methoxy radicals along with the known RO–H and RO–D bond strengths, the gas-phase acidities ($\Delta H°_{acid}$) of CD_3OD (383.9 ± 0.7 kcal/mol), CH_3OD (383.5 ± 0.7 kcal/mol), and CD_3OH (382.0 ± 0.7 kcal/mol) were calculated. A simple model is employed to predict reaction efficiencies and branching ratios for these isotope-exchange reactions.

I. Introduction

One of the goals of gas-phase ion chemistry is to determine intrinsic reactivities and thermochemistry in order to provide a fuller understanding of solution chemistry. A particularly powerful tool toward this end is to employ cluster ions and investigate the effects of solvation as solvent is added to a reaction, one molecule

0002-7863/90/1512-6832$02.50/0

at a time. Eventually, one may hope to approach the effects observed in liquids and so "bridge the gap" between solution and gas phase. One largely unexplored area of gas-phase ion chemistry is the effect of deuterium substitution on reactivity and bond strength. In this paper we examine these isotope effects in the negative ion clusters of methoxide with methanol ($CH_3O^-\cdot HOCH_3$). We have studied a series of 12 bimolecular isotope-exchange reactions of these solvated ions (eqs 1–12) for which

$$CH_3O^-\cdot HOCH_3 + CH_3OD \rightarrow CH_3O^-\cdot DOCH_3 + CH_3OH \quad (1)$$

$$CH_3O^-\cdot DOCH_3 + CH_3OH \rightarrow CH_3O^-\cdot HOCH_3 + CH_3OD \quad (2)$$

$$CH_3O^-\cdot HOCH_3 + CD_3OH \rightarrow CH_3O^-\cdot HOCD_3 + CH_3OH \quad (3)$$

$$CH_3O^-\cdot HOCD_3 + CH_3OH \rightarrow CH_3O^-\cdot HOCH_3 + CD_3OH \quad (4)$$

$$CH_3O^-\cdot DOCH_3 + CD_3OD \rightarrow CH_3O^-\cdot DOCD_3 + CH_3OD \quad (5)$$

$$CH_3O^-\cdot DOCD_3 + CH_3OD \rightarrow CH_3O^-\cdot DOCH_3 + CD_3OD \quad (6)$$

$$CH_3O^-\cdot DOCD_3 + CD_3OD \rightarrow CD_3O^-\cdot DOCD_3 + CH_3OD \quad (7)$$

$$CD_3O^-\cdot DOCD_3 + CH_3OD \rightarrow CH_3O^-\cdot DOCD_3 + CD_3OD \quad (8)$$

$$CD_3O^-\cdot HOCD_3 + CD_3OD \rightarrow CD_3O^-\cdot DOCD_3 + CD_3OH \quad (9)$$

$$CD_3O^-\cdot DOCD_3 + CD_3OH \rightarrow CD_3O^-\cdot HOCD_3 + CD_3OD \quad (10)$$

$$CH_3O^-\cdot HOCD_3 + CD_3OH \rightarrow CD_3O^-\cdot HOCD_3 + CH_3OH \quad (11)$$

$$CD_3O^-\cdot HOCD_3 + CH_3OH \rightarrow CH_3O^-\cdot HOCD_3 + CD_3OH \quad (12)$$

a unique ionic product exists. In addition we have determined the branching ratios for two isotope-exchange reactions (eqs 13 and 14), which have several possible ionic products. For these

$$CH_3O^-\cdot HOCH_3 + CD_3OD \rightarrow CH_3O^-\cdot DOCH_3 + CD_3OH \quad (13a)$$

$$\rightarrow CH_3O^-\cdot HOCD_3 + CH_3OD \quad (13b)$$

$$\rightarrow CH_3O^-\cdot DOCD_3 + CH_3OH \quad (13c)$$

$$CD_3O^-\cdot DOCD_3 + CH_3OH \rightarrow CH_3O^-\cdot HOCD_3 + CD_3OD \quad (14a)$$

$$\rightarrow CH_3O^-\cdot DOCD_3 + CD_3OH \quad (14b)$$

$$\rightarrow CD_3O^-\cdot HOCD_3 + CH_3OD \quad (14c)$$

investigations, we employed the recently constructed tandem flowing afterglow-selected ion flow tube (FA-SIFT), which has been described previously.[1] This instrument is particularly useful because the ion source allows us to produce and mass select isotopically labeled cluster ions with ease as described in section II. The ions are then injected into the pristine environment of the flow tube, free of interfering neutral precursors and other ions.

Section III discusses the known thermochemistry of the methoxide–methanol system, the ion–neutral collision rate coefficients and a simple quasi-equilibrium model that relates thermodynamics and reaction efficiencies.

Section IV presents our experimental results including heats of reaction, heats of formation, and bond strengths for the cluster ions as a function of deuteration. We then use these values to estimate reaction efficiencies and compare them with experimental values. Finally, we use the model discussed in section III to predict experimental branching ratios. In section V we discuss the implications of these data and compare our results with those of previous workers.

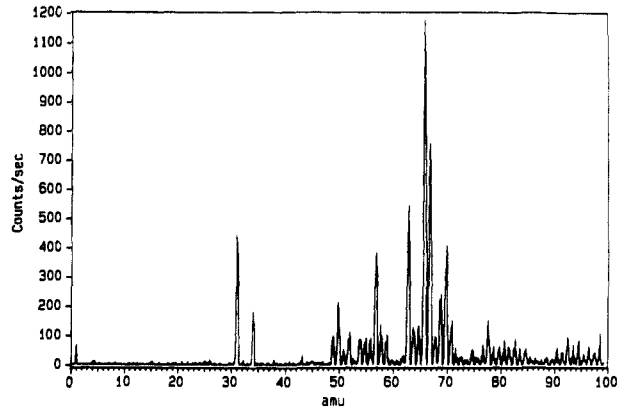

Figure 1. Mass spectrum of ions formed in the flowing afterglow ion source from electron impact on N_2O followed by reaction with CH_4, CH_3OH, and CD_3OD.

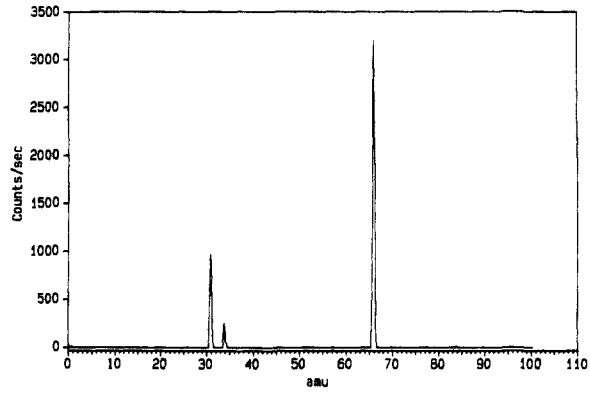

Figure 2. Mass spectrum of injected $CH_3O^-\cdot HOCD_3$. CH_3O^- and CD_3O^- result from collision-induced dissociation of $CH_3O^-\cdot HOCD_3$.

II. Experimental Section

The methoxide–methanol cluster ions are generated in the flowing afterglow source of the tandem FA-SIFT by a sequence of ion–molecule reactions. Hydroxide ion is produced by dissociative electron attachment to N_2O (forming O^-) followed by rapid hydrogen atom abstraction from methane. Reaction of hydroxide with methanol produces methoxide ions, which undergo subsequent association with methanol to form $CH_3O^-\cdot(HOCH_3)_n$. The desired cluster ion is mass selected from all other ions by the quadrupole mass filter and injected into the second flow tube for further study. Different forms of deuterated reactant ions are made by using the appropriately deuterated neutral reagents.

Figure 1 shows the mass spectrum that results when deuterated and undeuterated reagents are present in the flowing afterglow source and all ions are injected into the second flow tube and detected downstream. When the SIFT quadrupole mass filter is tuned to m/z 66, the $CH_3O^-\cdot HOCD_3$ ion is selected and injected, as shown in Figure 2. Some collision-induced dissociation of this ion to form CH_3O^- and CD_3O^- is evident at masses 31 and 34, respectively. These ions, however, do not interfere with studies of the cluster ion reactions; the three-body association reactions of the unsolvated ions are considerably slower than the bimolecular exchange reactions of the cluster ions.[2] The ions undergo 10^4 or more collisions with the helium buffer gas before reaction with neutral reagents and are thus expected to be at thermal equilibrium.

This source also allows preparation of $^{13}CH_3O^-$ from unenriched precursors. When no deuterated reagents are present in the flowing afterglow source, mass selection of m/z 64 corresponds to $CH_3O^-\cdot HOCH_3$ ions that contain a single carbon-13 label. Upon injection into the second flow tube at slightly elevated kinetic energy, collision-induced dissociation generates approximately equal amounts of CH_3O^- and

(1) Van Doren, J. M.; Barlow, S. E.; DePuy, C. H.; Bierbaum, V. M. *Int. J. Mass Spectrom. Ion Processes* **1987**, *81*, 85.

(2) Most of the ions formed by collision-induced dissociation will react with the neutral reagents by proton/deuteron transfer rather than association. From the measured extent of fragmentation and known rate coefficients for all processes, we can calculate that collision-induced dissociation followed by association reactions will perturb rate coefficients and branching ratios measured in this study by less than 2%.

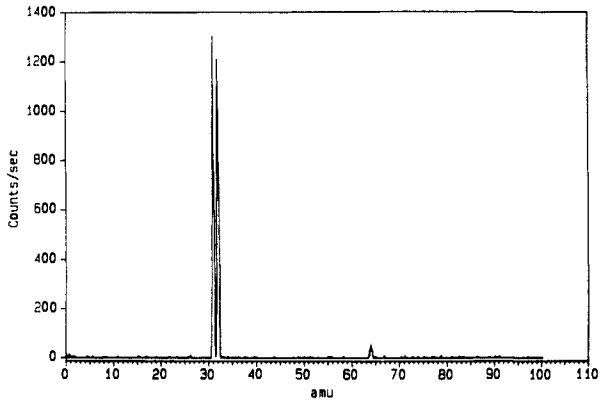

Figure 3. Mass spectrum of collision-induced dissociation of $^{13}CH_3O^-{\cdot}HOCH_3$.

$^{13}CH_3O^-$, as shown in Figure 3. The small difference in intensity between m/z 31 and 32 is not meaningful as the relative intensities fluctuate slightly for different spectra. This method of producing $^{13}CH_3O^-$ precludes contamination at m/z 32 by O_2^-. It is interesting to note that the equal intensities of CH_3O^- and $^{13}CH_3O^-$ reflect equal stabilities of these ions while the predominance of CH_3O^- relative to CD_3O^- in Figure 2 reflects its lower basicity; the proton preferentially departs with the more basic anion. This phenomenon has been previously demonstrated by Wright et al.[3]

Reaction rate coefficients are measured by monitoring the decrease of reactant ion as a function of reaction distance. Neutral reagent flow rates are determined by measuring the pressure change in a calibrated volume system. Product ion branching ratios are found by extrapolation to zero reaction distance. Since all cluster ions monitored in this experiment occur in a narrow mass range (m/z 63–70), mass discrimination effects are expected to be minimal.

The experiments are performed at room temperature and helium pressures of ~0.5 Torr. Reagent purities are as follows: CH_3OH (99.9%), CH_3OD (99.5%), CD_3OH (99.0%), CD_3OD (99.8%), He (99.995%). Freeze–pump–thaw cycles are used to degas the liquid samples; the helium buffer gas is passed through a molecular sieve trap immersed in liquid nitrogen.

III. Background

In this section we present background material necessary fo a detailed understanding of the results presented in section IV Subsection A gives the heats of formation for several of the ion and neutral molecules studied and these provide the basis of th thermochemical conclusions below. Subsection B discusses ion molecule collision rates, which are critical for the interpretatio of this work. Subsection C presents the equations employed fo relating thermochemical and kinetic data.

A. Thermochemistry. The heats of formation for several ions and neutral molecules in this experiment may be found or deduced from sources in the literature.[4-11] These values are summarized in Table Ia. The heats of formation of the deuterated analogues of methanol, for example, CH_3OD, can be derived from reactions such as eq 15. In this reaction the heats of formation of CH_3OH,

$$CH_3OH + D_2 \rightarrow CH_3OD + HD \quad (15)$$

D_2, and HD are known and the reaction enthalpy is determined from the differences in zero-point energies.[12,13] Once the heats of formation for the various deuterated methanols are known, the heat of formation of CD_3O^- can be determined from data given by Grabowski et al.[14]

Table I

(a) Heats of Formation of Ions and Neutrals

species	ΔH_f,[a] kcal/mol	source
H^+	365.7	Lias et al.[7]
D^+	366.6	Lias et al.[7]
H_2	0.0	definition
HD	0.08	Chase et al.[6]
D_2	0.0	definition
CH_3O^-	−32.3 ± 0.4	see text
CD_3O^-	−34.8 ± 0.4	Grabowski et al.[14] (see text)
CH_3OH	−48.2 ± 0.1	Pedley et al.[10]
CH_3OD	−49.1 ± 0.1	Shimanouchi[13] (see text)
CD_3OH	−51.1 ± 0.1	Shimanouchi[13] (see text)
CD_3OD	−52.1 ± 0.1	Shimanouchi[13] (see text)
$CH_3O^-{\cdot}HOCH_3$	−109.3 ± 2.6	Meot-Ner and Sieck[4,9]

(b) Gas-Phase Acidities of Methanol and Deuterated Methanols

species	$\Delta H°_{acid}$,[b] kcal/mol	source
CD_3OD	383.9 ± 0.7	see text
CH_3OD	383.5 ± 0.7	see text
CD_3OH	382.0 ± 0.7	see text
CH_3OH	381.6 ± 0.7	Meot-Ner and Sieck[9]

[a] Where error bars are not listed, they are <0.05 kcal/mol. [b] Error bars are absolute total error, relative uncertainties are ±0.1 kcal/mol.

Table Ib shows the various deuterated methanols listed in order of increasing acidity. The gas-phase acidity of AH is defined as the enthalpy change ($\Delta H°_{acid}$) for reaction 16. Since the heats

$$AH \rightarrow A^- + H^+ \qquad \Delta H_{rxn}^{298} = \Delta H°_{acid} \quad (16)$$

of formation of reactants and products are known in each case (see Table Ia), the acidities can be directly calculated.

Another way of obtaining the $\Delta H°_{acid}$ is to use a thermochemical cycle[15] such as indicated in eqs 17–20. The acidity order

$$AH \rightarrow A^\bullet + H^\bullet \qquad \Delta H = DH(A\text{-}H) \quad (17)$$

$$A^\bullet + e^- \rightarrow A^- \qquad \Delta H = -EA(A^\bullet) \quad (18)$$

$$H^\bullet \rightarrow H^+ + e^- \qquad \Delta H = IP(H^\bullet) \quad (19)$$

$$\Delta H°_{acid} = DH(A\text{-}H) + IP(H^\bullet) - EA(A^\bullet) \quad (20)$$

of the deuterated methanols is determined by three factors: the RO–H (or RO–D) bond dissociation energy, the electron affinity of the alkoxy radical, and the ionization potentials of H or D (313.59 and 313.67 kcal/mol, respectively).[6] The difference in acidity of CH_3OH and CD_3OH is primarily due to the difference in the electron affinities of CH_3O and CD_3O since the RO–H bond dissociation energies are the same to within 0.02 kcal/mol.[13] The electron affinities are 36.20 ± 0.51 and 35.79 ± 0.51 kcal/mol for CH_3O and CD_3O, respectively;[16,17] thus, CH_3O^- is the more stable, less basic anion and CH_3OH is more acidic than CD_3OH by 0.4 kcal/mol. The same argument can be applied to CH_3OD and CD_3OD. In contrast, the acidity difference between CH_3OH

(3) Wright, L. G.; McLuckey, S. A.; Cooks, R. G.; Wood, K. V. *Int. J. Mass Spectrom. Ion Phys.* **1982**, *42*, 115.
(4) Meot-Ner, M.; Sieck, L. W. *J. Am. Chem. Soc.* **1986**, *108*, 7525.
(5) Caldwell, G.; Rozeboom, M. D.; Kiplinger, J. P.; Bartmess, J. E. *J. Am. Chem. Soc.* **1984**, *106*, 4660.
(6) Chase, M. W.; Davies, C. A.; Downey, J. R.; Frurip, D. J.; McDonald, R. A.; Syverud, A. N. *JANAF Thermochemical Tables*, 3rd ed. *J. Phys. Chem. Ref. Data* **1985**, *14*, Suppl. 1.
(7) Lias, S. G.; Bartmess, J. F.; Liebman, J. F.; Holmes, J. L.; Levin, R. D.; Mallard, W. G. Gas-Phase Ion and Neutral Thermochemistry. *J. Phys. Chem. Ref. Data* **1988**, *17*, Suppl. 1.
(8) Benson, S. W. *Thermochemical Kinetics*, 2nd ed.; J. Wiley: New York, 1976; p 296.
(9) Meot-Ner, M.; Sieck, L. W. *J. Phys. Chem.* **1986**, *90*, 6687.
(10) Pedley, J. B.; Naylor, R. D.; Kirby, S. P. *Thermochemical Data of Organic Compounds*; Chapman and Hall: New York, 1986.
(11) Mackay, G. I.; Rakshit, A. B.; Bohme, D. K. *Can. J. Chem.* **1982**, *60*, 2594.
(12) Herzberg, G. *Molecular Spectra and Molecular Structures. II. Infrared and Raman Spectra of Polyatomic Molecules*; Van Nostrand: New York, 1945; p 528.
(13) Shimanouchi, T. *Tables of Molecular Vibrational Frequencies*; NSRDS NBS 39; National Bureau of Standards: Washington, DC, 1972.
(14) Grabowski, J. J.; DePuy, C. H.; Van Doren, J. M.; Bierbaum, V. M. *J. Am. Chem. Soc.* **1985**, *107*, 7384.
(15) Bartmess, J. E.; McIver, R. T., Jr. *Gas Phase Ion Chemistry*; Bowers, M. T., Ed.; Academic Press, Inc.; New York, 1979; Vol. 2, p 89.
(16) Engleking, P. C.; Ellison, G. B.; Lineberger, W. C. *J. Chem. Phys.* **1978**, *69*, 1826.
(17) The electron affinity is the difference in energy between the lowest vibrational states of the neutral and the ion. As discussed in ref 16, the hydrogens are more constrained in CH_3O than in CH_3O^-, resulting in a higher zero-point energy in the neutral methoxy radical than in the ion. Therefore, when the species are deuterated, the zero-point energy of the neutral decreases more than the zero-point energy of the ion. Thus, the energy gap between the neutral and ion (i.e., the electron affinity) is smaller for the deuterated than undeuterated species.

Table II. Ion–Molecule Reduced Collision Rate Coefficient: $A^- + CH_3OH$

method	k,[a] 10^{-9} cm^3 amu$^{1/2}$/s
Langevin[18]	4.2
ADO[19]	7.6
statistical adiabatic channel[21]	10.3
variational transition state[20]	10.2
experimental average (see text)	9.3 (±0.8)

[a] To calculate the collision rate coefficient, divide the reduced rate coefficient by the square root of the reduced mass.

and CH_3OD arises primarily from the difference in bond dissociation energies. The OD bond dissociation energy in CH_3OD is 1.8 kcal/mol higher than the OH bond dissociation energy[13] in CH_3OH; thus, including the slight difference in ionization potentials between H and D, CH_3OH is a stronger acid than CH_3OD by 1.9 kcal/mol. When the acidities of CH_3OD and CD_3OH are compared, differences in bond dissociation energies, electron affinities, and ionization potentials must be considered. The OD bond dissociation energy is 1.8 kcal/mol higher than the OH bond dissociation energy, the CH_3O electron affinity is 0.4 kcal/mol higher than the CD_3O electron affinity, and the ionization potential of D is 0.1 kcal/mol higher than the ionization potential of H; thus, we find that CD_3OH is a stronger acid than CH_3OD by 1.5 kcal/mol. It is satisfying to note that the kinetic data of Grabowski et al.[14] give the same values to within 0.1 kcal/mol.

B. Ion–Molecule Collision Rate Coefficients and Reaction Efficiencies. Ion–molecule collision rates are of particular interest because, as will be shown in the next section, one may deduce thermochemical information from reaction efficiencies. We consider five models for the collision rate: the Langevin[18] model, the average dipole orientation (ADO)[19] model, variational transition state theory (VTST)[20], the statistical adiabatic channel (SAC)[21] model, and an empirical method.

All of these theories have two things in common: first, contributions due to the structure or identity of the ions are ignored; second, the predicted rates are proportional to $\mu^{-1/2}$, where μ is the reduced mass of the colliding species. It is, therefore, useful to define a "reduced collision rate coefficient" for a specific neutral molecule, which is simply the collision rate coefficient multiplied by the square root of the reduced mass. Table II provides a comparison of the reduced collision rate coefficient for methanol based upon these various theoretical models. Also included in Table II is an estimate based on experimental results. Here we have taken the average reduced rate coefficient of 12 rapid ion–molecule reactions[22-25] given in the literature, as well as our own values for eqs 21 and 22. This latter value compares favorably

$$NH_2^- + CH_3OH \rightarrow CH_3O^- + NH_3 \qquad k = 2.6\ (\pm 0.1) \times 10^{-9}\ \text{cm}^3/\text{s} \quad (21)$$

$$N^+ + CH_3OH \rightarrow \text{products} \qquad k = 2.8\ (\pm 0.1) \times 10^{-9}\text{cm}^3/\text{s} \quad (22)$$

to the literature value of 3.1×10^{-9} cm^3/s from Adams et al.[26] The average experimental value lies in the midrange of those deduced from the most commonly employed theories. We have therefore adopted this empirical value for determining reaction efficiencies in this work and we assume that deuterium substitution in methanol does not affect the collision rate beyond changing the mass. It is clear from Table II that employing either VTST or SAC rate coefficients would produce only small differences in our conclusions.

During the course of this investigation we measured a rate coefficient for eq 23 that proved to be smaller than anticipated.

$$^{13}CH_3O^- + CH_3OH \rightarrow CH_3O^- + {}^{13}CH_3OH \qquad k = 8.1\ (\pm 0.5) \times 10^{-10}\ \text{cm}^3/\text{s} \quad (23)$$

This thermoneutral proton-transfer reaction might be expected to proceed at half the collision rate whereas the measured efficiency is only ~35%.[27] Brauman[28] has also observed a reduced efficiency for this reaction. This may result from a significant barrier for proton transfer in the proton bound dimer. Alternatively, the low efficiency may result from some ionic attack at the unreactive methyl group; if then a significant barrier to rearrangement of the collision complex exists, we would also observe a loss of reaction efficiency. Su et al.[29] recently discussed the requirement of proper orientation of ion–molecule trajectories for the formation of reactive complexes in S_N2 processes.

A similar slowing of proton- and deuteron-transfer reactions is observed in the data of Grabowski et al.[14] These workers examined, among other things, the exchange reactions $CH_3O^- + CD_3OH \rightleftharpoons CD_3O^- + CH_3OH$ and $CH_3O^- + CD_3OD \rightleftharpoons CD_3O^- + CH_3OD$. If we use the reported values for the reaction rates and the value for the collision rate discussed above, we find the "total" reaction efficiency, i.e., forward plus reverse, to be 0.71 and 0.64, respectively; this may be compared with 0.70 found from reaction 23 by assuming the reverse rate is equal to the forward one. For reactions without barriers, the sum of forward and reverse reaction efficiencies is unity. Thus, these simple proton- or deuteron-transfer processes of unsolvated methoxide ions appear to possess a barrier on the reaction surface.

C. Relating Thermochemical and Kinetic Data. For the methoxide–methanol-exchange reactions studied in this work (Table III), thermochemical information is deduced from the ratios of the forward and reverse rate coefficients. We can make a simplifying approximation owing to the great similarity of reactants and products, and the fact that none of the reactions is extremely exothermic or endothermic: the ratio of the partition functions of products and reactants will very nearly cancel in the rate expression; thus, apart from a reaction path degeneracy factor correction, we have assumed that $\Delta G \approx \Delta H$.

The importance of barriers in exchange reactions of solvated methoxide ions is unknown. However, if no significant barriers exist along the reaction path, apart from the rotational barrier associated with the ion–dipole complex formation, and provided no other angular momentum effects occur, it is then a simple matter to modify the Olmstead–Brauman formulation[30] to calculate reaction efficiencies. When this is done, we obtain exactly the results we would expect from simple thermodynamic considerations. We find for endothermic reactions that the reaction efficiency (or probability), $P_{en}(T)$, is given by eq 24, where η_r and

$$P_{en}(T) = \frac{\exp(-\Delta H/kT)}{\eta_r/\eta_f + \exp(-\Delta H/kT)} \quad (24)$$

η_f are the reaction path degeneracy factors for the reverse (back to reactants) and forward (on to products) reactions, respectively. An identical result is obtained for the reaction efficiency for exothermic reactions. In the next section we show that this simple

(18) Langevin, P. M. *Ann. Chem. Phys.* **1905**, *5*, 245.
(19) Su, T.; Bowers, M. T. *Int. J. Mass Spectrom. Ion Phys.* **1975**, *17*, 309.
(20) Chesnavich, W. J.; Su, T.; Bowers, M. T. *J. Chem. Phys.* **1980**, *72*, 2641.
(21) Troe, J. *Chem. Phys. Lett.* **1985**, *122*, 425.
(22) Albritton, D. L. *Atomic Data Nucl. Data Tables* **1978**, *22*, 1.
(23) Ikezoe, Y.; Matsuoka, S.; Takebe, M.; Viggiano, A. *Gas Phase Ion–Molecule Reaction Rate Constants Through 1986*; Maruzen: Tokyo, 1987.
(24) Anicich, V. G.; Huntress, W. T. A Survey of Bimolecular Ion–Molecule Reactions for Use in Modeling the Chemistry of Planetary Atmospheres, Cometary Comae and Interstellar Clouds. Jet Propulsion Laboratory, 1986.
(25) The 12 reactions include those of methanol with CH^+, CH_2^+, N^+ (two values), NH^+, NH_2^+, CH_4^+, H_3O^+ (two values), CN^+, CO^+, NCO^+ (two values), H_2CO^+, and C_3H^+.
(26) Adams, N. G.; Smith, D.; Paulson, J. F. *J. Chem. Phys.* **1980**, *72*, 288.
(27) Although the experimental efficiency of 35% and the theoretical efficiency of 50% are similar, we believe that the difference is significant: the rate coefficient was measured with high precision and the experimental efficiency is <50% with any of the collision models of Table II (except Langevin, which is not applicable). In constrast, reaction efficiencies of 50% have been measured for the Cl^- + HCl system: Van Doren, J. M.; DePuy, C. H.; Bierbaum, V. M. *J. Phys. Chem.* **1989**, *93*, 1130.
(28) Brauman, J., private communication.
(29) Su, T.; Morris, R. A.; Viggiano, A. A.; Paulson, J. F. *J. Phys. Chem.*, in press.
(30) Olmstead, W. N.; Brauman, J. I. *J. Am. Chem. Soc.* **1977**, *99*, 4219.

Table III. Rate Coefficients and Reaction Enthalpies

reaction	k, 10^{-10} cm^3/s	ΔH, kcal/mol
1. $CH_3O^-{\cdot}HOCH_3 + CH_3OD \rightarrow CH_3O^-{\cdot}DOCH_3 + CH_3OH$	5.56 ± 0.72	0.47 ± 0.11
2. $CH_3O^-{\cdot}DOCH_3 + CH_3OH \rightarrow CH_3O^-{\cdot}HOCH_3 + CH_3OD$	12.3 ± 1.6	
3. $CH_3O^-{\cdot}HOCH_3 + CD_3OH \rightarrow CH_3O^-{\cdot}HOCD_3 + CH_3OH$	10.4 ± 0.7	0.28 ± 0.08
4. $CH_3O^-{\cdot}HOCD_3 + CH_3OH \rightarrow CH_3O^-{\cdot}HOCH_3 + CD_3OH$	8.33 ± 0.98	
5. $CH_3O^-{\cdot}DOCH_3 + CD_3OD \rightarrow CH_3O^-{\cdot}DOCD_3 + CH_3OD$	11.3 ± 1.3	0.21 ± 0.13
6. $CH_3O^-{\cdot}DOCD_3 + CH_3OD \rightarrow CH_3O^-{\cdot}DOCH_3 + CD_3OD$	8.08 ± 1.55	
7. $CH_3O^-{\cdot}DOCD_3 + CD_3OD \rightarrow CD_3O^-{\cdot}DOCD_3 + CH_3OD$	5.47 ± 0.25	0.07 ± 0.05
8. $CD_3O^-{\cdot}DOCD_3 + CH_3OD \rightarrow CH_3O^-{\cdot}DOCD_3 + CD_3OD$	12.4 ± 0.9	
9. $CD_3O^-{\cdot}HOCD_3 + CD_3OD \rightarrow CD_3O^-{\cdot}DOCD_3 + CD_3OH$	4.40 ± 0.63	0.44 ± 0.12
10. $CD_3O^-{\cdot}DOCD_3 + CD_3OH \rightarrow CD_3O^-{\cdot}HOCD_3 + CD_3OD$	9.29 ± 1.29	
11. $CH_3O^-{\cdot}HOCD_3 + CD_3OH \rightarrow CD_3O^-{\cdot}HOCD_3 + CH_3OH$	5.21 ± 0.56	0.09 ± 0.08
12. $CD_3O^-{\cdot}HOCD_3 + CH_3OH \rightarrow CH_3O^-{\cdot}HOCD_3 + CD_3OH$	12.1 ± 1.0	

Table IV. Heats of Formation and Hydrogen Bond Strengths of Methoxide–Methanol Clusters

species	ΔH_f,[a] kcal/mol	ΔH_B,[a] kcal/mol
$CH_3O^-{\cdot}HOCH_3$	−109.3[b]	28.8[b]
$CH_3O^-{\cdot}DOCH_3$	−109.7 ± 0.1	28.3 ± 0.1
$CH_3O^-{\cdot}HOCD_3$	−111.9 ± 0.1	28.5 ± 0.1
$CH_3O^-{\cdot}DOCD_3$	−112.5 ± 0.1	28.1 ± 0.1
$CD_3O^-{\cdot}HOCD_3$	−114.8 ± 0.1	28.9 ± 0.1
$CD_3O^-{\cdot}DOCD_3$	−115.4 ± 0.1	28.5 ± 0.1

[a] Stated uncertainties are due to this experiment only and do not reflect the absolute uncertainty. [b] See Table I.

relationship generally produces very good agreement with our experimental results for methoxide–methanol clusters. This suggests that reaction barriers are less important for solvated than for unsolvated methoxide ions.

IV. Results and Analysis

A. Thermochemistry. Table III summarizes the rate coefficients for six pairs of reactions, each pair being nominally a forward (endothermic) and reverse (exothermic) reaction. Also shown in Table III is the reaction enthalpy for each pair. The rate coefficients for reactions 3, 5, 8, and 12 were divided by 2 before ΔH was calculated to account for the fact that the reactant ion had two exchangeable CH_3 (or CD_3) groups (the reaction path degeneracy correction). The error bars on the reaction rate coefficients and ΔH reflect the statistical uncertainty of the measurements. We estimate the absolute uncertainty of the rate coefficient measurements to be ±20%; however, the relative uncertainty between the measurements should be reflected by the statistical errors.

The heats of formation of the various deuterium-substituted methoxide–methanol dimers can be determined from the data in Tables I and III and these values are indicated in Table IV. It should be noted that the uncertainty in these values reflects only the additional uncertainty that these measurements bring to the values and not the absolute uncertainty, which rests in the data of Table I. Table V summarizes the effects on the methoxide–methanol bond strengths of substituting deuterium for hydrogen in the cluster ions.

B. Kinetics. The reaction efficiencies may be modeled as described in section IIIC. The results for both the endothermic and exothermic reactions are presented in Table VI. There is relatively good agreement between calculated and experimental reaction efficiencies except for reactions 9 and 10, which involve the substitution of the bridging H for D when two CD_3 groups are present.

This sort of analysis may be readily extended to model branching ratio measurements as well. In Table VIIa we show the results of a branching ratio experiment where all of the reactions are endothermic and we find good agreement between the quasi-equilibrium model and experiment. On the other hand, Table VIIb summarizes the data of an exothermic branching ratio measurement where the modeling produces only fair agreement. These results and their implications will be discussed in the following section.

Table V. Comparisons of Cluster Ion Bond Strengths

stronger bond	weaker bond	change in bond strength, kcal/mol
(a) replacing H with D		
$CH_3O^-{\cdot}HOCH_3$	$CH_3O^-{\cdot}DOCH_3$	0.5
$CH_3O^-{\cdot}HOCD_3$	$CH_3O^-{\cdot}DOCD_3$	0.4
$CD_3O^-{\cdot}HOCD_3$	$CD_3O^-{\cdot}DOCD_3$	0.4
(b) replacing CH_3OH (or CH_3OD) with CD_3OH (or CD_3OD)		
$CH_3O^-{\cdot}HOCH_3$	$CH_3O^-{\cdot}HOCD_3$	0.3
$CH_3O^-{\cdot}DOCH_3$	$CH_3O^-{\cdot}DOCD_3$	0.2
(c) replacing CH_3O^- with CD_3O^-		
$CD_3O^-{\cdot}HOCD_3$	$CH_3O^-{\cdot}HOCD_3$	0.4
$CD_3O^-{\cdot}DOCD_3$	$CH_3O^-{\cdot}DOCD_3$	0.4

Table VI. Comparison of Calculated and Experimental Reaction Efficiencies

rxn pair (Table III)	ΔH,[a] kcal/mol	η_f[a]	η_r[a]	P_{en}[b] % calcd	P_{en}[b] % exptl	P_{ex}[c] % calcd	P_{ex}[c] % exptl
1, 2	0.47	1	1	31	28	69	61
3, 4	0.28	2	1	56	53	44	42
5, 6	0.21	2	1	58	58	42	41
7, 8	0.07	1	2	31	29	69	63
9, 10	0.44	1	1	32	23	68	48
11, 12	0.09	1	2	30	27	70	61

[a] Enthalpies and reaction path degeneracies are listed for the endothermic direction (odd-numbered reactions of Table III). For the exothermic direction (even-numbered reactions of Table III), the sign of ΔH is reversed and η_f and η_r are interchanged. [b] Reaction efficiency for the endothermic direction (odd-numbered reactions of Table III). [c] Reaction efficiency for the exothermic direction (even-numbered reactions of Table III).

V. Discussion

A. Heats of Reaction. Reactions 1 and 2 have been previously studied both at lower pressures in an ICR by Weil and Dixon[31] and at higher pressures, in a high-pressure mass spectrometer, by Szulejko et al.[32] Our equilibrium constant (K = 0.45) for reactions 1 and 2 lies between the values obtained by Weil and Dixon[31] (K = 0.31) and Szulejko et al.[32] (K = 0.60). Considering the differences among the three experiments, the agreement is reasonably good. Weil and Dixon[31] also modeled the methoxide–methanol dimers computationally; in these studies, Weil and Dixon[31] calculated and reported the normal-mode frequencies for both $CH_3O^-{\cdot}HOCH_3$ and $CH_3O^-{\cdot}DOCH_3$. Using the normal mode frequencies, they calculated an equilibrium constant, K = 0.35, which is in good agreement with the experimental values.

(31) Weil, D. A.; Dixon, D. A. *J. Am. Chem. Soc.* **1985**, *107*, 6859.
(32) Szulejko, J. E.; Wilkinson, F. E.; McMahon, T. B. A High Pressure Mass Spectrometric Determination of Equilibrium Isotope Effects of Association and Exchange Reactions of F^- and RO^- with Simple OH/OD Labelled Alcohols. Proceedings of the 37th ASMS Conference on Mass Spectrometry and Allied Topics, Miami Beach, FL, May 21–26, 1989.

Table VII. Kinetic Analysis of a Branching Ratio

experimental results	branching ratio, calcd	branching ratio, exptl	ΔH, kcal/mol
(a) Endothermic Reactions			
13a. $CH_3O^-\cdot HOCH_3 + CD_3OD \rightarrow CH_3O^-\cdot DOCH_3 + CD_3OH$	0.22	0.20 ± 0.03	0.6
13b. $\rightarrow CH_3O^-\cdot HOCD_3 + CH_3OD$	0.60	0.60 ± 0.03	0.4
13c. $\rightarrow CH_3O^-\cdot DOCD_3 + CH_3OH$	0.18	0.20 ± 0.05	0.7
(b) Exothermic Reactions			
14a. $CD_3O^-\cdot DOCD_3 + CH_3OH \rightarrow CH_3O^-\cdot HOCD_3 + CD_3OD$	0.35	0.55 ± 0.05	−0.4
14b. $\rightarrow CH_3O^-\cdot DOCD_3 + CD_3OH$	0.36	0.35 ± 0.05	0.0
14c. $\rightarrow CD_3O^-\cdot HOCD_3 + CH_3OD$	0.29	0.10 ± 0.03	−0.3

Scheme I

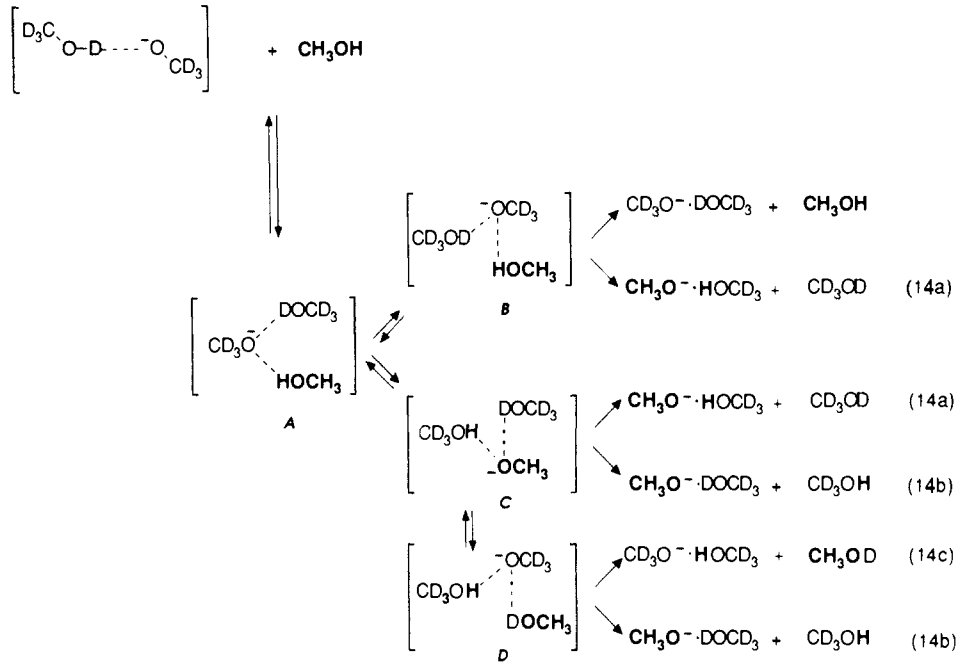

B. Hydrogen Bonding. In addition to the ion–dipole and ion–induced dipole attractive forces, the energy of adduct formation also includes contributions from hydrogen bonding. Since the first two terms are essentially identical for any of the combinations of ion and ligand in Table III, we may interpret the changes in bond energy, ΔH_B (Tables IV and V), as changes in the hydrogen bonding. The problems associated with describing and understanding this phenomenon have received considerable experimental and theoretical attention over the years, especially in the liquid phase, and a number of reviews and books are available.[33] However, most of these treatments refer to neutral–neutral hydrogen bonding rather than the ion–neutral cases considered here.

In the gas phase the differences in the bond strengths of various deuterated methoxide–methanol cluster ions can be understood by examining the acidity of the neutral molecule and the basicity of the anion involved in the cluster. Table V compares the bond strengths of similar pairs of the clusters. Substituting an H with D at the bridging position (Table Va) weakens the methoxide–methanol bond by ~0.4 kcal/mol. Similarly, substituting CH_3 in the neutral methanol with CD_3 (Table Vb) weakens the methoxide–methanol bond by 0.2–0.3 kcal/mol. For these comparisons the anion remains unchanged; however, these substitutions result in the incorporation of a weaker acid into the cluster. This weaker acid allows less donation of its proton or deuteron to the anion and the hydrogen bond is weakened.

In contrast, replacing CH_3 in the methoxide anion with CD_3 (Table Vc) strengthens the methoxide–methanol bond. For these comparisons, the neutral methanol remains unchanged but the basicity of the anion is increased. The stronger hydrogen bond results from the increased ability of the anion to interact with the acidic site of the methanol.

The greater strength of the hydrogen bond relative to the deuterium bond as illustrated in Table Va has precedent in solution studies of methanol. Bonner[34] has measured infrared spectra of pure CH_3OH and CH_3OD and of varying concentrations of these methanols in carbon tetrachloride solution. He has concluded that hydrogen bonding is more extensive than deuterium bonding in these systems. Our results indicate that the greater strength of the hydrogen bond is an intrinsic property and not a result of solvation. Equilibrium isotope effects in solvated gaseous anions have also been probed by Dixon and co-workers[35] and Larson and McMahon.[36,37] In the $CH_3CH_2O^-\cdot HOCH_2CH_3$,[35] $F^-\cdot H_2O$,[36] $Cl^-\cdot H_2O$,[36] and $Cl^-\cdot HCl$[37] systems, hydrogen bonding is consistently found to be stronger than deuterium bonding.

C. Reaction Efficiencies, Branching Ratios, and Mechanism. Table VI summarizes calculated and experimental reaction efficiencies for reactions 1–12. With the exception of reaction pair 9 and 10, the sums of the forward and reverse experimental efficiencies are close to unity, spanning the range 0.88–0.99. Moreover, the individual forward and reverse efficiencies are in

(33) (a) *The Hydrogen Bond: Recent Developments in Theory and Experiments*; Schuster, P., Zundel, G., Sandorfy, C., Eds.; North-Holland: Amsterdam, 1976. (b) Kay, B. D. Dynamics, Energetics, and Structure of Hydrogen Bonded Clusters: Elucidating the Transition from the Gaseous to the Condensed State, Ph.D. Thesis, University of Colorado, Boulder, 1982. (c) Joesten, M. D.; Shaad, J. L. *Hydrogen Bonding*; M. Dekker: New York, 1974. (d) Vinogradov, S. N.; Linnell, R. H. *Hydrogen Bonding*; Van Nostrand Reinhold: New York, 1971. (e) Pimentel, G. C.; McClellan, A. *The Hydrogen Bond*; Reinhold: New York, 1960.

(34) Bonner, O. D. *J. Chem. Thermodyn.* **1970**, *2*, 577.

(35) Ellenberger, M. R.; Farneth, W. E.; Dixon, D. A. *J. Phys. Chem.* **1981**, *85*, 4.

(36) Larson, J. W.; McMahon, T. B. *J. Am. Chem. Soc.* **1988**, *110*, 1087.

(37) Larson, J. W.; McMahon, T. B. *J. Phys. Chem.* **1987**, *91*, 554.

good agreement with values calculated by the methods of section IIIC. These results suggest that the collision complexes are sufficiently long-lived for extensive energy randomization to occur and that, at most, only small barriers exist along the reaction path. The formation of ion–dipole complexes is expected to occur along an attractive surface without barriers; within these complexes, however, two types of barriers are possible, as discussed above: (A) complexes with the proper reactive orientation, i.e., with bonding at the proton, may have barriers along the proton-transfer path; (B) complexes with an unreactive orientation, i.e., with bonding at the methyl group, may have barriers along the path of cluster rearrangement. These barriers will differ in reactions of solvated and unsolvated ions; the increased complexity of the ion–dipole complexes of solvated reactant ions may make these barriers less important than for the unsolvated species. The specific origin of the slowing of reactions 9 and 10 is not understood. However, we are dealing with very subtle differences of the potential energy surface and the small changes in energetics as the reaction is successively deuterated may be sufficient to make these subtleties detectable.

The branching ratio measurements are particularly interesting. In Table VIIa, we show the effects of having only endothermic reaction channels. Here the complex is apparently quite long-lived and nearly complete energy randomization has occurred, i.e., we can predict the branching ratios from thermodynamic considerations alone. When exothermic channels occur, as shown in Table VIIb, the picture changes considerably. In this case the branching ratios are controlled by both the thermodynamics and the kinetics. That is, in cases where several rearrangement steps are required, the reaction is less likely to occur, even if it is thermodynamically favored, because with each step of the rearrangement process, an exothermic dissociation process is possible. This is the most probable explanation for the high measured value for reaction 14a, which requires only one step, and low measured value for reaction 14c, which requires two or three steps. Our results therefore indicate that for exothermic reactions complete equilibration of the collision complex does not occur under our experimental conditions. In Scheme I we illustrate a qualitative mechanism to show how this stepwise rearrangement could occur. In this scheme the reactant ion is represented as an asymmetrical cluster in which the bridging deuteron is localized on one of the deuteriomethoxy groups; this is presumably the lowest energy structure although deuteron transfer between the CD_3O groups should be relatively facile. Upon reaction of this ion with unlabeled methanol, an intermediate A is formed in which CD_3O^- interacts electrostatically with both deuterated and undeuterated methanol. Deuteron transfer to CD_3O^- generates intermediate B, whereas proton transfer forms C. In the dissociation of complex B, CD_3O^- can bond to either CD_3OD (which regenerates reactants) or to CH_3OH, an exothermic process (14a). Similarly, complex C can decompose by association of CH_3O^- with CD_3OH in an exothermic reaction (14a) or with CD_3OD in a thermoneutral process (14b). Alternatively, complex C can rearrange by intramolecular deuteron transfer from CD_3OD to CH_3O^- to generate intermediate D. This complex can dissociate by both an exothermic channel to form $CD_3O^-\cdot HOCD_3$ (14c) and a thermoneutral pathway to form $CH_3O^-\cdot DOCD_3$ (14b). It is clear from this scheme that although channels 14a and 14c are both favored thermodynamically, the latter channel is inhibited since more extensive rearrangements are required; when competing exothermic pathways are possible, equilibrium is not achieved within the reaction complex for these systems.

VI. Conclusions

We have examined the methoxide–methanol cluster as a function of deuterium substitution and determined the relative heats of formation and cluster bond strengths. These effects can be understood by examining the relative acidities of the neutral ligand and the basicities of the anions. The good agreement between our data and the quasi-equilibrium model may be taken as an indication that our intuition about the potential energy surfaces is qualitatively correct. That is, ion–neutral molecule collisions lead to complex formation without a barrier. Further, the barriers to proton transfer and complex rearrangement must lie well below the energy of the separated reactants.

This work provides a natural starting point for the consideration of a number of related questions and in the future we hope to explore several of them. In particular we wish to investigate the effects of higher order clusters of methanol as well as other hydrogen bonded clusters—particularly the hydroxide–water and methoxide–water systems. We are also interested in pursuing the analogous cationic systems and in studying the formation of gas-phase clusters in the flow tube.

Acknowledgment. We gratefully acknowledge support of this work by the National Science Foundation under Grant CHE-8815446. We thank Charles DePuy, Scott Gronert, and Stephen Prodnuk for valuable discussions.

Registry No. CH_3O^-, 3315-60-4; $HOCH_3$, 67-56-1; D, 7782-39-0; CD_3OD, 811-98-3; CH_3OD, 1455-13-6; CD_3OH, 1849-29-2.